International Journal of
INTELLIGENT SYSTEMS AND APPLICATIONS IN ENGINEERING
ISSN:2147-6799 www.ijisae.org Original Research Paper

An Intelligent method of analysis of Magnetic Resonance Images (MRI), X-Ray and CT Images for Abnormality Identification.

[1]Kalaiah J. B., [2]S. N. Chandrashekara

Submitted: 11/01/2024 **Revised**: 17/02/2024 **Accepted**: 25/02/2024

Abstract: The efficient and accurate interpretation of biomedical imaging data, including Computed Tomography (CT), X-ray, and Magnetic Resonance Imaging (MRI), is crucial for the diagnosis, treatment planning, and management of various diseases. This study aims to develop and validate advanced computational models for the automated analysis of CT, X-ray, and MRI images to improve diagnostic accuracy and efficiency. By employing machine learning and deep learning techniques, our models are trained and tested on a comprehensive dataset of biomedical images to identify and classify pathological features across different conditions.

In this work, we focus on the evaluation metrics of True Positive (TP), True Negative (TN), False Positive (FP), and False Negative (FN) rates, alongside derived statistical measures such as Sensitivity (Recall rate), Specificity, Precision, SNR and PSNR and the F1 score to assess the performance of our models. Sensitivity measures the model's ability to correctly identify positive cases, while Specificity assesses its ability to exclude negative cases accurately. Precision evaluates the proportion of true positive results in all positive predictions, and the F1 score provides a harmonic mean of Precision and Sensitivity, offering a balance between them for a comprehensive performance metric. Our findings demonstrate that the integration of proposed methodology significantly enhances the model's capability to accurately distinguish between pathological and non-pathological cases across CT, X-ray, and MRI modalities. The models exhibit high Sensitivity and Specificity, indicating reliable identification of disease presence and absence. Furthermore, the Precision and F1 scores highlight the models' accuracy and balanced performance in diagnostic predictions. The implications of this study are profound, offering a pathway towards the development of automated diagnostic tools that can support radiologists and healthcare practitioners in making more accurate, efficient, and consistent diagnostic decisions. By leveraging the quantitative analysis of TP, TN, FP, and FN rates, along with key performance metrics such as Sensitivity, Specificity, Precision, and F1 score, our research contributes to the ongoing efforts in improving patient outcomes through enhanced diagnostic imaging analysis.

Keywords: *outcomes, diagnostic, X-ray, MRI, comprehensive, integration*

1. Introduction.

The process of viewing the interior of the body for therapeutic and clinical purposes is known as biomedical imaging. Biomedical imaging is the complex process of taking, analyzing, and displaying structural or functional images of living things or systems, as well as extracting and processing data from the images. Biomedical imaging helps identify anomalies in the human anatomy. Among the biomedical imaging technologies are computed tomography (CT), magnetic resonance imaging (MRI), positron emission tomography (PET), ultrasound, and x-rays. Biomedical image characteristics are not visible to radiologists with the unaided eye. By combining several machine learning algorithms, Computer-Aided Detection (CAD) plays a significant role in feature detection. It speaks of pattern recognition that finds elements that are questionable in images that aren't immediately apparent. CAD can be used to diagnose a wide range of abnormalities, including brain tumours, breast cancer, and pulmonary nodules on the chest. CAD uses computer-generated output to diagnose problems. Image pre-processing, segmentation, feature extraction, and classification are the several stages of a computer-aided design process. With CAD, diagnosis times will be shortened, radiologists' workloads will be reduced, diseases that are hidden from view will be found, and human mistake rates will drop. [1]

Any instability, including abnormal cell division and growth in the fundamental body components, leads to abnormality. It is possible for a collection of abnormal cells to directly damage good cells. The existence of the tumor may be the cause. These abnormalities become dangerous and have a big effect on the standard of human health. Biomedical imaging allows radiologists to identify a broad spectrum of abnormalities in the human body. Various methods are employed by biomedical imaging devices to obtain images.[2]

Types of Biomedical images Biomedical imaging is concerned with the acquisition of images for diagnostic and therapeutic applications. Biomedical imaging started from the invention of X-rays in 1895, and it is also used

[1]*Research Scholar, R & D,Dept of CSE,SJCIT Affiliated to VTU Belagavi Asst.prof. Dept.of ECE,J V Institute of Technology, Bidadi Karnataka, India kalaiahjb@gmail.com.*
[2]*Prof & Head Dept. of CSE C Byregowda institute of Technology Kolar, Karnataka, India*
snc_chandru@yahoo.co.in

to research biological structure and function as well as to answer fundamental biomedical problems. Figure 1 shows different biomedical imaging machines, their output images, and the technique used to make the image.[18]

Computed Tomography The word ”tomography” comes from the Greek words ”tomos,” which means ”slice” or ”section,” and ”graphe,” which means ”drawing.” The CT imaging system creates cross-sectional images of anatomy, sometimes known as ”slices,” which are utilized for 2 diagnostic and therapeutic purposes. It is a computerized X-ray imaging technology in which a thin beam of X-rays is targeted at a patient and quickly circulates the body, producing signals, and these signals are processed by the computer attached to the CT machine to create the cross-sectional images of the body[19]. The CT computer employs advanced mathematical procedures to produce a 2D image slice of the patient every time the X-ray source completes one full revolution. Thickness of the tissue shown in each imaging slice varies with each CT machine; however, it commonly falls between 1 -10 millimetres. From the CT, the doctors can see the image slices individually or can be stacked together to produce the 3D image of the patient’s organ. Using this method, the radiologist or doctor can rotate the 3D image or view the organ slice by slice, making it easier to locate and analyze the abnormality.[17] CT scans can be used to identify disease or injury within various parts of the body[20]. It can be used to detect tumors or lesions within the abdomen and locate injuries, tumours, clots leading to stroke, hemorrhage, and other conditions in the brain. It can also be used to detect lung abnormalities, detect bone fractures, bone tumors, etc. [3][4]

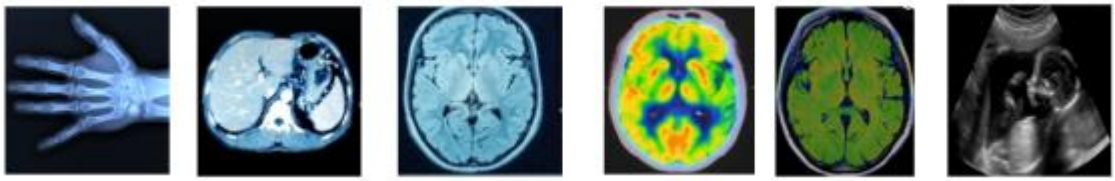

Fig 1. Various bio medical images.

Imaging Using Magnetic Resonance A non-invasive imaging method that produces detailed three-dimensional anatomy images is magnetic resonance imaging (MRI). It's widely used to identify illnesses, make diagnoses, and monitor their progression.[15] It is predicated on a technology that excites three and senses shifts in the orientation of protons' rotational axis in the water that constitutes biological tissues. Protons in the body are forced to align with the intense magnetic field created by MRI's powerful magnets. When the patient receives pulses of radiofrequency current, the protons become activated and spin out of balance, straining against the force of the magnetic field. When the radiofrequency field is turned off, the energy released as the protons realign with the magnetic field may be detected by the MRI sensors. The surroundings and the chemical structure of the molecules affect how much energy is produced and how long it takes for the protons to realign with the magnetic field.[16] Before or during an MRI, a patient may receive intravenous contrast agents—which usually contain the element Gadolinium—to quicken the pace at which protons realign with the magnetic field. The rate at which the protons realign determines the image's brightness. For imaging soft tissues and other non-bony parts of the body, MRI scanners are very useful. [5]

2. Objectives of Research.

The objective of addressing these challenges is to develop advanced computational tools and algorithms that can automate the analysis of MRI, X-ray, and CT images. [6] Improved consistency and accuracy in image interpretation, reducing the variability associated with human error. Enhanced detection of subtle pathological features, facilitating early diagnosis and treatment. Efficient handling and analysis of large imaging datasets, improving the scalability of diagnostic processes.

3. Problem Statement.

In the realm of medical diagnostics, the accuracy and efficiency of interpreting biomedical images such as Magnetic Resonance Imaging (MRI), X-rays, and Computed Tomography (CT) scans are paramount for early detection, diagnosis, and treatment planning of various diseases and injuries. Despite significant advancements in medical imaging technologies, several challenges persist that limit the potential of these diagnostic tools. These challenges include:

High Variability in Image Interpretation: The interpretation of MRI, X-ray, and CT images heavily relies on the expertise of radiologists. Variability in experience and subjective judgment among practitioners can lead to inconsistencies in diagnosis, affecting patient outcomes.[7]

Limited Accessibility to Expert Analysis: In many regions, especially rural and underserved areas, there is a shortage of skilled radiologists. This limitation hinders timely and accurate diagnosis, delaying the initiation of appropriate treatment plans.[8]

Increasing Volume of Imaging Data: The growing reliance on biomedical imaging for diagnostics has led to an exponential increase in the volume of imaging data. Managing, storing, and analysing this vast amount of data pose significant logistical and computational challenges.[9]

Detection of Subtle Pathological Features: Early stages of diseases or small lesions can be difficult to detect, and sometimes subtle abnormalities are overlooked. This oversight can lead to delayed treatment with potentially adverse outcomes for patients.[10]

Integration of Multimodal Imaging Data: Different imaging modalities (MRI, X-ray, CT) provide complementary information. However, integrating and correlating data from these diverse sources to improve diagnostic accuracy and patient care remains a complex challenge.[11]

4. Proposed Algorithm.

The figure 2., interprets the generic representation of the proposed algorithm, which includes five different iterations with the point of data collection to comparative analysis by involving the basic steps of the image processing on the three different set of database such as MRI,CT and X-Ray images under consideration, the brief description of the proposed steps are as follows:

1.Data Collection:

Collect a comprehensive dataset consisting of CT, X-ray, and MRI image samples annotated with disease presence or absence.

2.Pre-Processing and Analysis:

Apply pre-processing techniques to enhance image quality. Utilize appropriate image analysis algorithms to identify features indicative of disease.

3.Model Training and Validation:

Train machine learning or deep learning models on a portion of the dataset. Validate the models on a separate portion of the dataset to avoid overfitting.

4.Performance Evaluation:

For each imaging modality (CT, X-ray, MRI), compute the TP, TN, FP, and FN by comparing the model predictions against the ground truth annotations. Calculate Sensitivity, Specificity, Precision, and F1 score based on the above metrics.

5.Comparative Analysis:

Compare the performance metrics across CT, X-ray, and MRI to evaluate their diagnostic effectiveness. Highlight the imaging modality that demonstrates superior performance in terms of Sensitivity, Specificity, Precision, and F1 score.

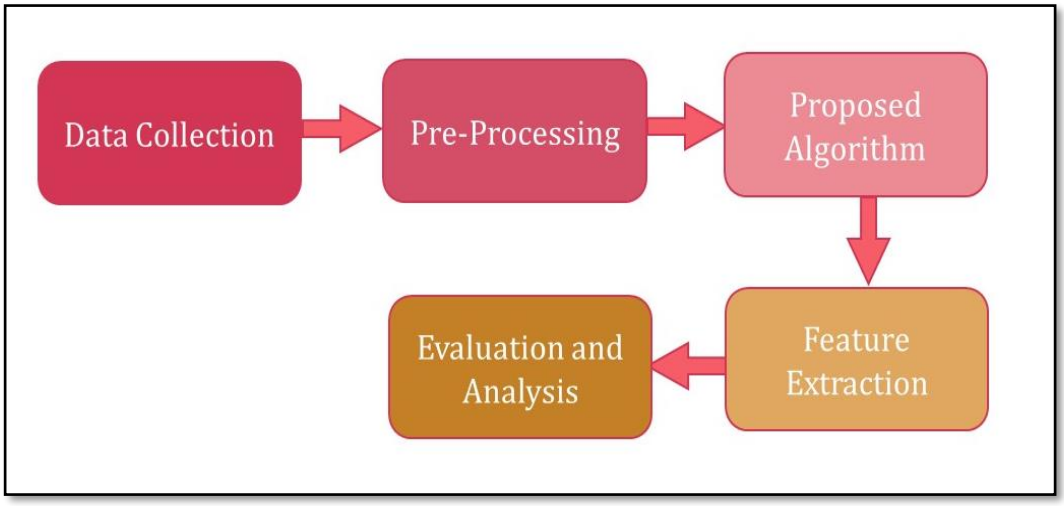

Fig 2: Proposed Block Diagram

5. Databases Under Consideration.

The databases are collected from the openly available data which are freely available for the research the MRI data is extracted from the http://datasets.datalad.org/?dir=/openfmri . The XRay image datasets are extracted from the http://www.cell.com/cell/fulltext/S0092-8674(18)30154-5 . the CT scan images are extracted from the database https://www.kaggle.com/datasets/kmader/siim-medical-images [12][13][14]

6. Results and Discussion.

The parameters used for measuring the system performance are F1 score, Sensitivity / Recall rate Specificity, Precision, PSNR, SNR. F1 score is a machine learning evaluation metric that measures a model's accuracy. It combines the precision and recall scores of a

model. The accuracy metric computes how many times a model made a correct prediction across the entire dataset. To compute F1 score first confusion matrix has to be computed. The confusion matrix has four essential components:

- True Positives (TP): Number of samples *correctly* predicted as "positive."
- False Positives (FP): Number of samples *wrongly* predicted as "positive."
- True Negatives (TN): Number of samples *correctly* predicted as "negative."
- False Negatives (FN): Number of samples *wrongly* predicted as "negative."

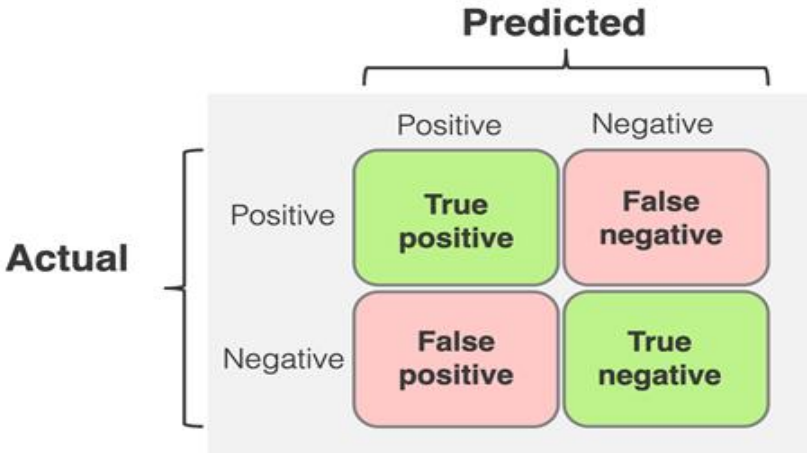

Fig 3: True Positive and True negative table

Using the components of the confusion matrix, various metrics are like precision, recall, and F1 score are defined.

$$Precision = \frac{TP}{TP+FP} \text{,,,,,,,,,,,,,,,,,,,,,,}(1)$$

$$Recall = \frac{TP}{TP+FN} \text{,,,,,,,,,,,,,,,,,,,,,,}(2)$$

$$F1\ Score = \frac{2(Precision)(Recall)}{Precision+Recall} \text{,,,,,,,,,,,,,,,,,,,,,,}(3)$$

Specificity measures the proportion of True Negative which are correctly identified by the model. It is also called a **True Negative Rate (TNR)**. The Sum of the True Negative Rate and False Negative Rate is 1. The higher Specificity of the model indicates that the model correctly identifies most of the negative results. A lower specificity value indicates the model misled the negative results as positive. In Medical terms, Specificity is a measure of the proportion of people not suffering from the disease who got predicted correctly as those not suffering from the disease.[21]

$$Specificity = \frac{TN}{TN+FP} \text{,,,,,,,,,,,,,,,,,,,,,,}(4)$$

Signal to Noise Ratio (SNR) in images indicates the signal quality found in an image. High SNR is required in many embedded vision applications, especially the ones which involve edge-based processing. Signal to Noise Ratio is defined as the ratio of mean value of the image to the standard deviation of the image and is given as, [22]

$$SNR = \frac{Mean}{Standard\ Deviation} \text{,,,,,,,,,,,,,,,,,,,,,,}(5)$$

Peak Signal to Noise Ratio (PSNR) is measured in decibels, between two images. This ratio is used as a quality measurement between the original and a reconstructed image. The higher the PSNR, the better the quality of the reconstructed image. PSNR is computed by using the following equation:

$$PSNR = 10log_{10}\frac{R^2}{MSE} \text{,,,,,,,,,,,,,,,,,,,,,,}(6)$$

R is the maximum fluctuation in the input image data type. For example, if the input image has a double-precision floating-point data type, then *R* is 1. If it has an 8-bit unsigned integer data type, *R* is 255, etc.[23]

$$MSE = \frac{\sum_{M,N}[I_1(m,n)-I_2(m,n)]^2}{M.N} \text{,,,,,,,,,,,,,,,,,,,,,,}(7)$$

MRI	CT-SCAN	X-RAY

Fig 4: Pre-processed input MR image.

The Figure-4 displays the input MRI considered for performing segmentation and tumor classification. The image is stored in the matrix $[I_m]_{630 \times 618}$ to perform further image analysis as a preliminary segmentation process.[24]

Initially, the system takes the pre-processed MR image as input values, which further goes through the process of multidimensional filtering operation. The usage of multidimensional filtering operation generates image 2D vector property, which is used to perform construction of the intensity variation vector-(IVV).[25] The term intensity variation refers to shape/spatial variation in terms of anatomical imbalance like tissues density or texture present in MR image. Therefore, the construction of IVV process provides a mechanism to perform detail analysis of input image to estimate and eliminate variation effects in the input image. Visual representation of the IVV is shown in Figure-5.

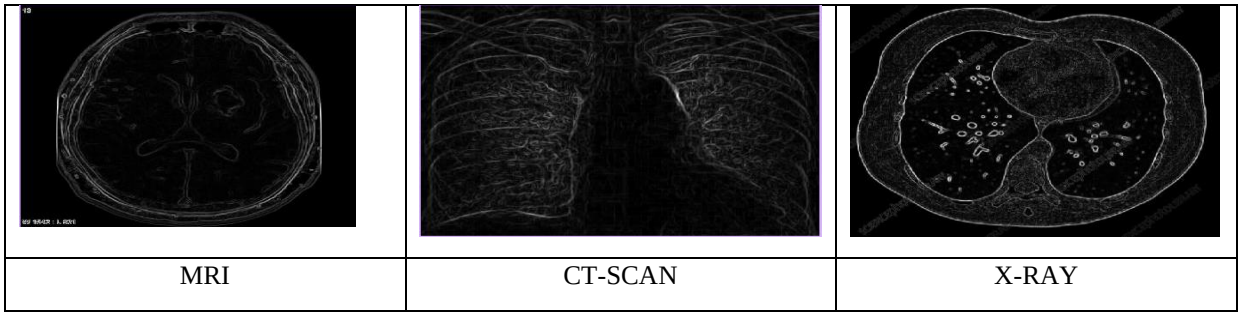

MRI	CT-SCAN	X-RAY

Fig 5: Visual representation of IVV

Due to the complex structure of the body organs, the MRI contains heterogeneous information. Therefore, the proposed system considers adopting a topographic mapping function to represent robust information about overall brightness and ridge of image. For this, the system watershed transform technique is used.[26] The watershed transform method is based on some uniformity principles like color, intensity or texture which helps to locate and identify objects or boundaries in the image by dividing the IVV into a set of pixels in the region. Thus, topographic mapping shown in the Figure-6 forms the initial segmentation of the image.

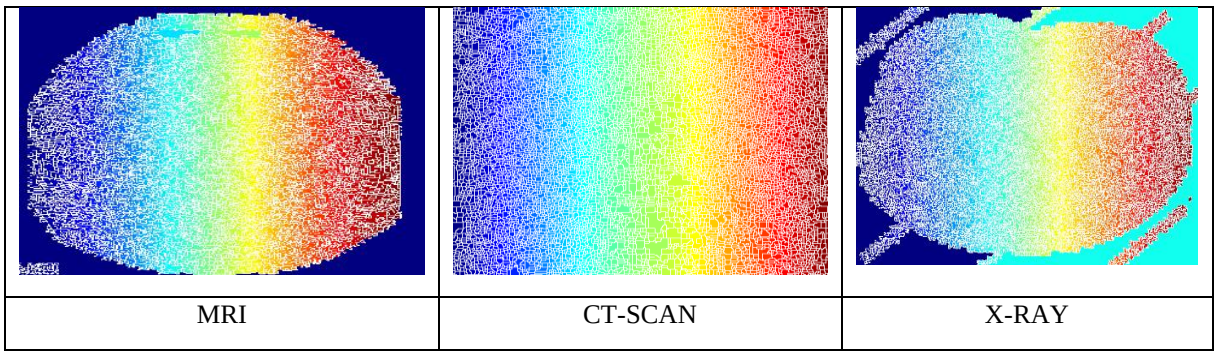

MRI	CT-SCAN	X-RAY

Fig 6: Topographic Mapping

The parameters that are similar on the basis of some homogeneity criteria such as color, intensity or texture, which helps to locate and identify objects or boundaries in an image that are similar on the basis of some homogeneity criteria such as color, intensity or texture, which helps to locate and identify objects or boundaries in

an image. After the successful execution of the above procedures, the value of achieved in terms of the label matrix. Actually, this performs a part of segmentation (region-based segmentation). This process converts the value of β_i into RGB representation to visualize the labelled region. Figure-7 demonstrates labelled segmentation of the MRI. [27]

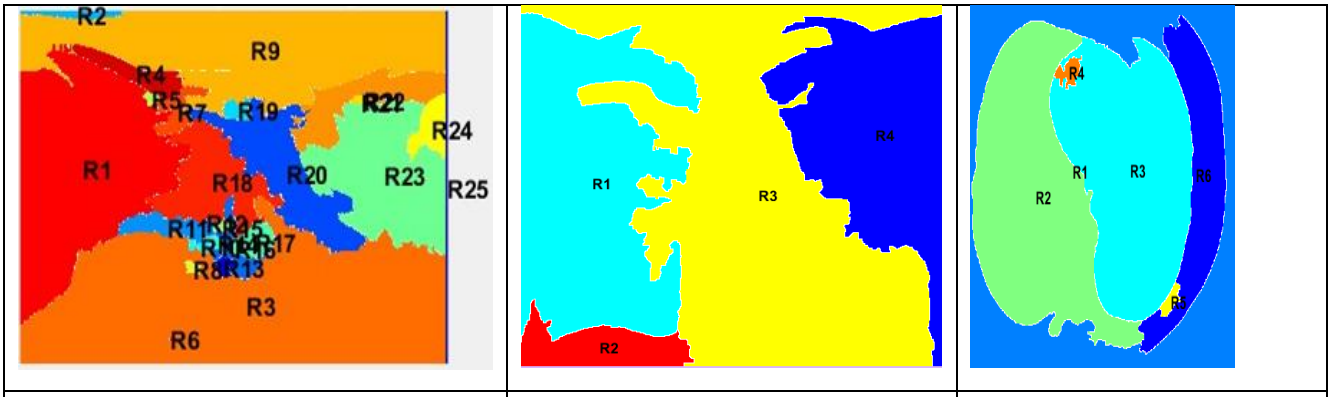

MRI	CT-SCAN	X-RAY

Fig 7: Labelled Topographic Representation of Indexed image

Next, morphological operations are performed to extract the regional maxima. The dilation operation on the image is computed to provide an expended size of an object of the image with smoothed structure.[32] The next step is to carry a complement of the image, which converts image area such as black area transforms into white and white area transform into black. Further, the system performs an operation to compute regional maxima of recently computed image. After this, the regional maxima (g_{mx}) is superimposed into the input image and is shown in the Figure-8. [28]

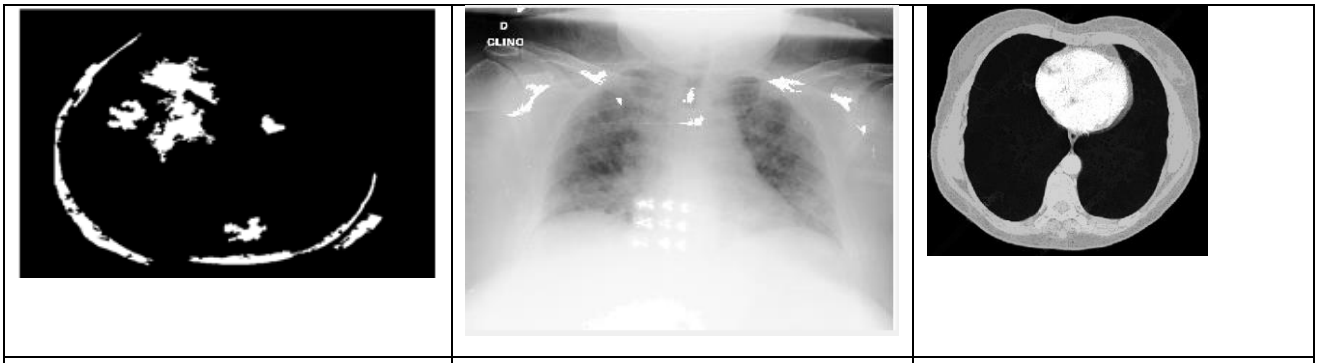

MRI	CT-SCAN	X-RAY

Fig 8: Regional Maxima of superimposed on the original image

The next step performs watershed transformation using similar function g_1 over the IVV to get the second version of the segmented image. For the visualization of the final output (β_2) of the segmented image in colour, the format is then achieved by using function g_2 over β_{i2}. This procedure gives another version of the segmented image (β_2).[29] Figure- illustrates colored segmented images as follows:

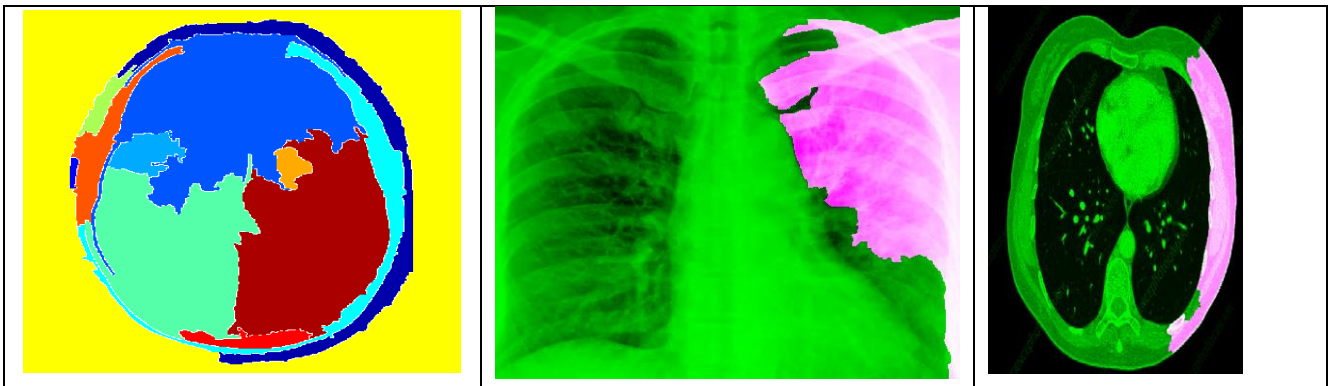

MRI	CT-SCAN	X-RAY

Fig 9: Colored segmented image

After this operation, maximum region matching is carried out from which suspicious is region is detected, and the tumor is identified in figure-9. The next process is to apply the ANN technique using function over the target vector and feature vector, which actually refers to the radial basis network.[31] A radial based network (Net) with the feature is assigned to a class variable which is initialized in the previous operation of feature extraction operation. Based on the region class, the system performs a binary decision-making process for flagging whether the tumor in the brain is malignant or benign. The next step computes the accuracy score in terms of multiple performance parameters. [30] Figure-10 shows the final result of the computed procedures for tumor detection form the MR image.

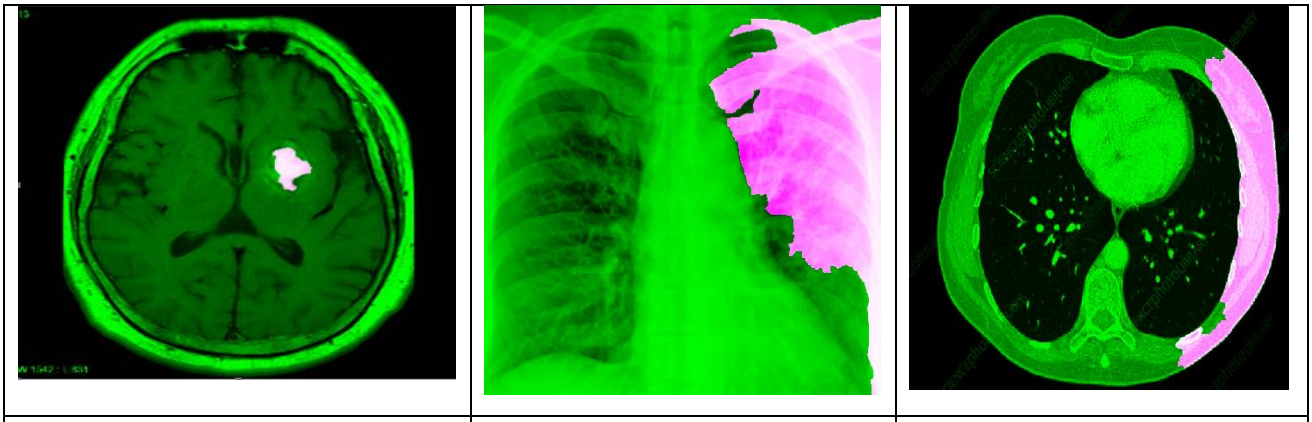

MRI	CT-SCAN	X-RAY

Fig 10: Detected Tumor in MRI

7. Results and Discussion.

Table 1 shows the summary of results for the ten different parameters under consideration for the three different types of image datasets under consideration in which two different images are considered in each type i.e., MRI, CT Scan and X Ray respectively.

Table1. summary of results for the parameters.

Parameter	MRI Image-1	MRI Image-2	CT Scan Image-1	CT Scan Image-2	X-Ray Image-1	X-Ray Image-2
TP	0.65116	0.885375	0.75116	0.80523	0.705116	0.81235
TN	0.99992	0.805206	0.802647	0.999106	0.999106	0.999106
FP	5.181e-05	0.194749	0.197353	0.000894	0. 000894	0. 000894
FN	0.34599	0.105402	0.254993	0.12548	0.45623	0.356987
Sensitivity	0.65302	0.893617	0.70223	0.745236	0.725636	0.85326
Specificity	0.9995	0.805242	0.802647	0.999106	0.999106	0.999106
Precision	0.99992	0.819698	0.752365	0.80635	0.689635	0.725486
F1 Score	0.79002	0.855063	0.824563	0.75235	0.68523	0.702523
SNR (dB)	55.6	58.6	50.8	52.5	41.2	42.35
PSNR (dB)	31.5	32.2	40.8	41.6	35.6	36.25

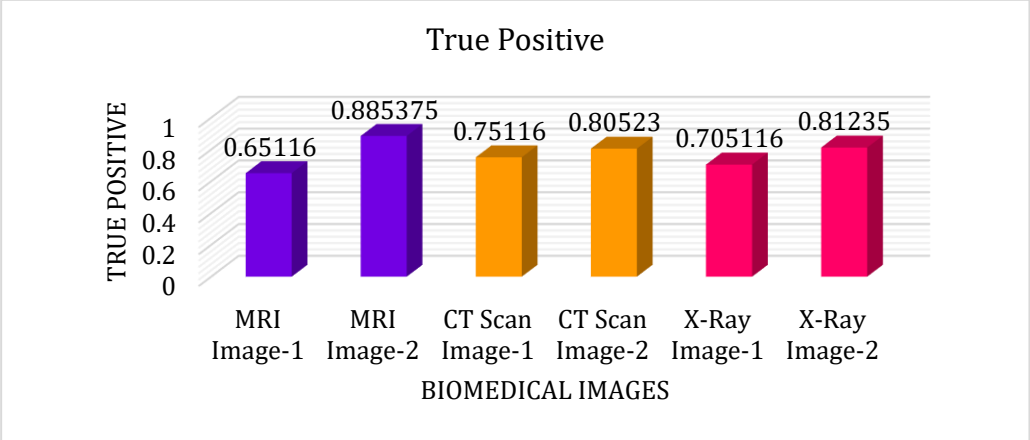

Fig 11: Plot of True Positive Values for MRI, CT scan and X-ray images

The figure 11, shows the plot of the True Positive values of the MRI images, CT scan and X-rays. As maximum for the MRI image, Whereas the true positive value is between the range of 0.7 to 0.8 for both X ray and CT scan images.

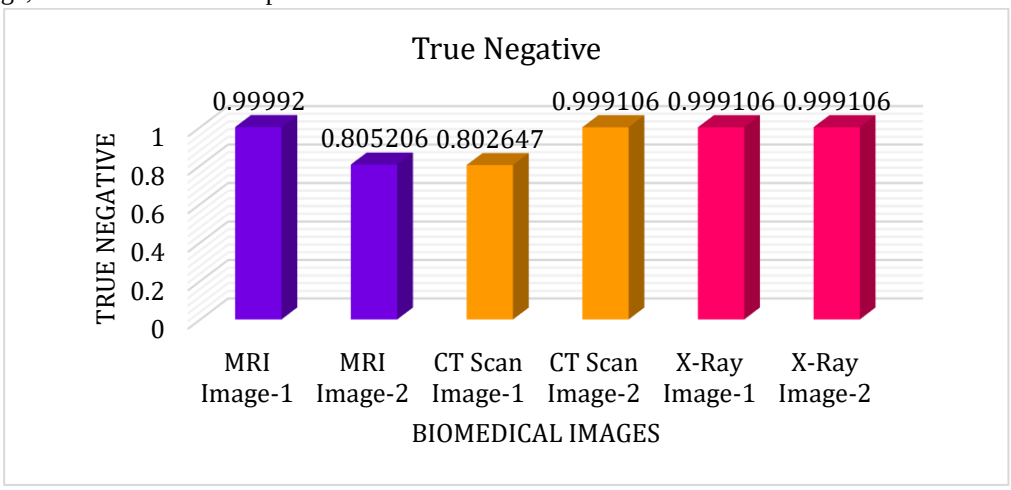

Fig 12: Plot of true negative values for MRI, CT scan and X-ray images

The above figure 12, shows the plotter true negative values obtained for for MRI, CT scan and X-ray images. From the plot, it is clear that for most of the images, the true negative value is approaching towards unity. The X-ray images show a consistent rate of true negative value. At the same time, there is a slight variation in the MRI image, and also CT scan image. The values of these images range from, 0.80 to 0.99.

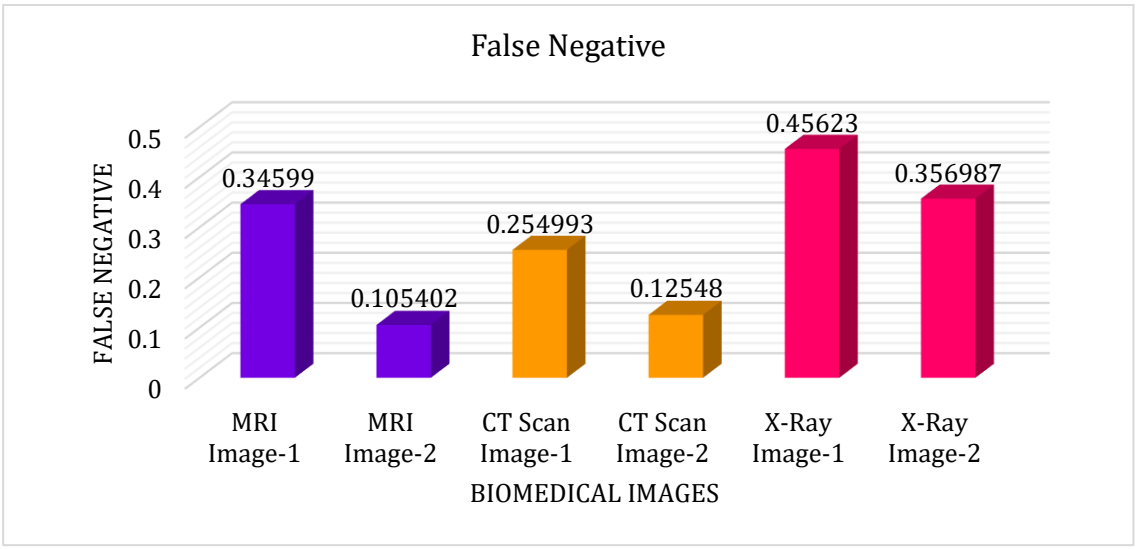

Fig 13: Plot of False negative values for MRI, CT scan and X-ray images

The above figure 13, shows the plot of false negative values in MRI, CT scan and X-ray images. The false negative values are less than 0.5 for all the categories of images. The ct scan image shows the average least value in false negative parameter.

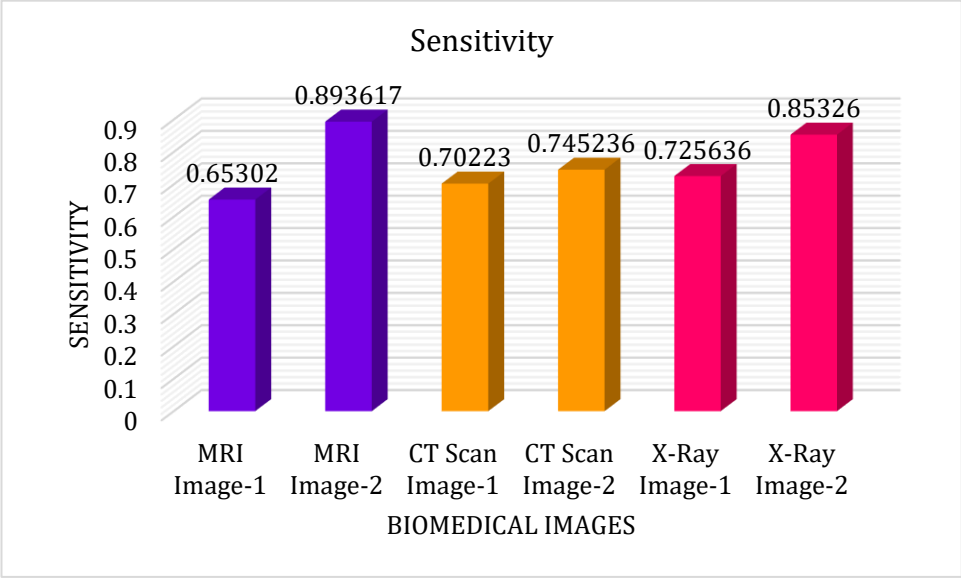

Fig 14: Plot of sensitivity for MRI, CT scan and X-ray images

The above figure 14 shows the plot of sensitivity for MRI, CT scan and X-ray images. The sensitivity for all the images lies above 0.6, It ranges from 0.6 to 0.9. There is an uniform distribution of the sensitivity for all Category of images taken.

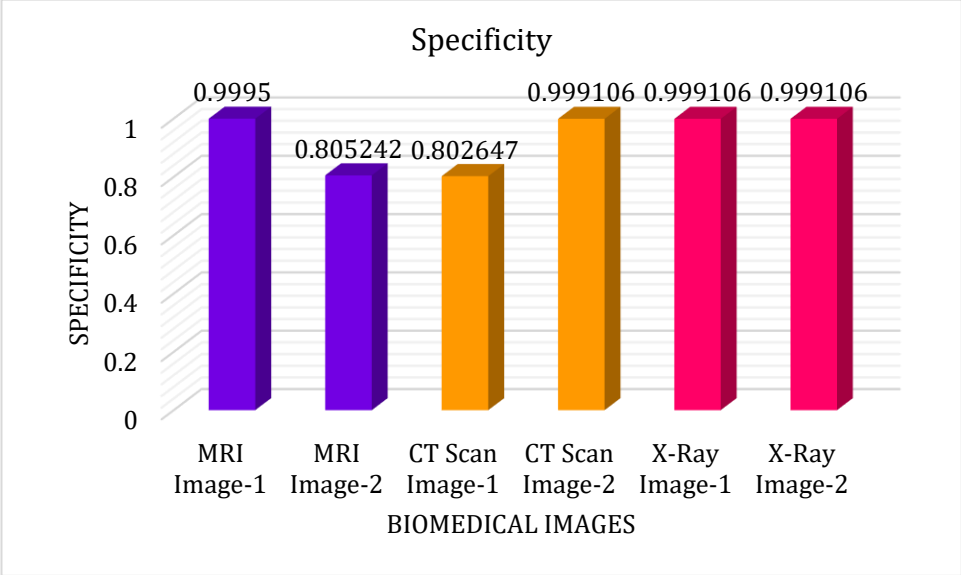

Fig 15: Plot of specificity for MRI, CT scan and X-ray images

The figure 15, shows the plot of specificity for MRI, CT scan and X-ray images. From the above plot, it can be clearly seen that for most of the images, the value of specificity is approaching towards unity. Among which the X-ray images clearly have the value of specificity reading unity. Whereas for MRI and CT scan images, it is ranging between 0.8 and 0.999.

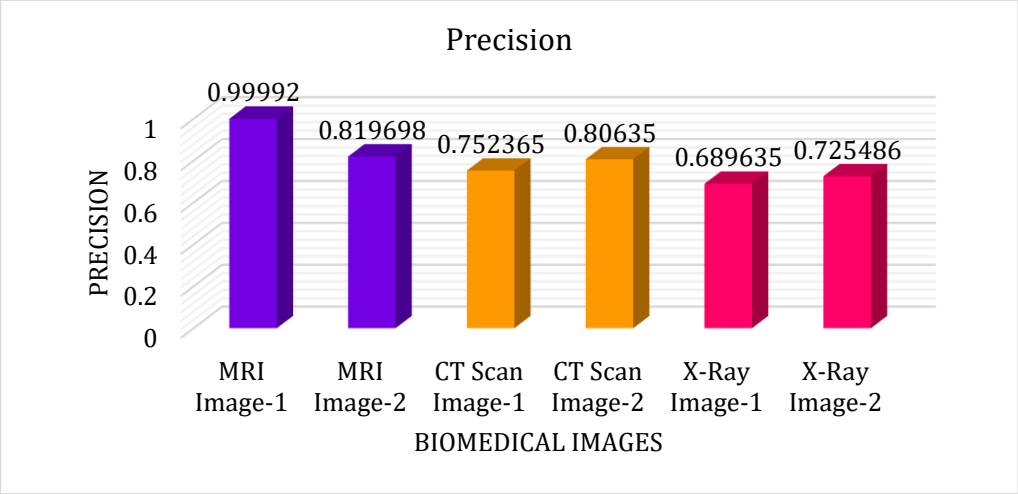

Fig 16: Plot of precision for MRI, CT scan and X-ray images

The above figure 16, shows the plot of precision for MRI, CT scan and X-ray images. Among the three categories of images MRI image shows the highest precision. Whereas the other two categories of images have the procession ranging from 0.6 to 0.8.

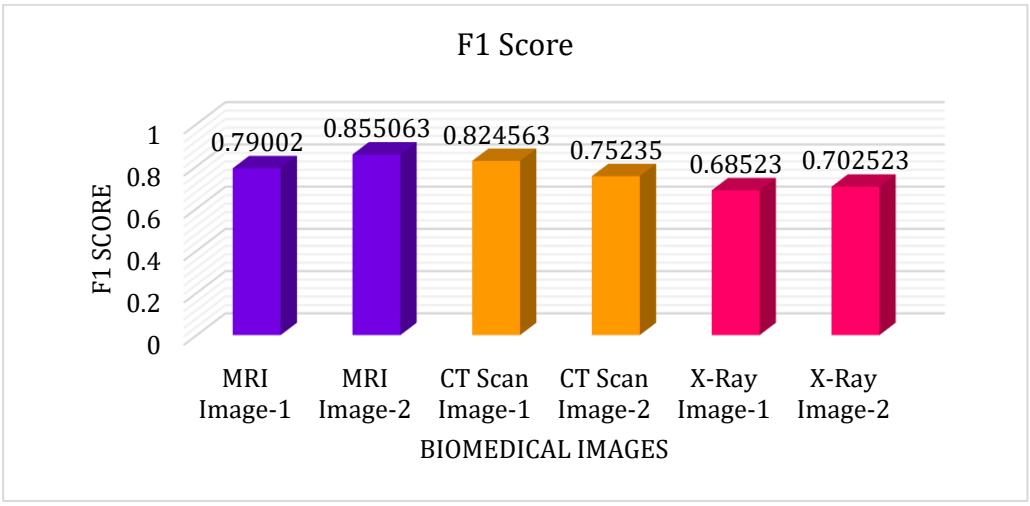

Fig 17: Plot of F1 score for MRI, CT scan and X-ray images

The figure 17, shows the plot of variation of F1 score for the different categories of biomedical images. The value of F1 score for all the category of images ranges from 0.68 to 0.85. The MRI image has the highest value and the least value is obtained by X ray images.

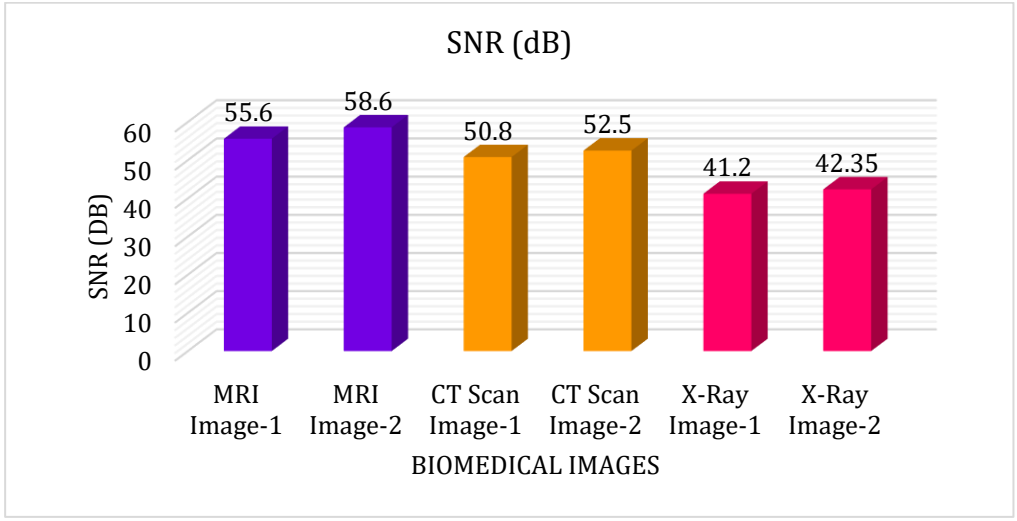

Fig 18: Plot of SNR for MRI, CT scan and X-ray images

The figure 18 shows the plot for SNR for MRI, CT scan and X-ray images. The SNR value for MRI images is better compared to CT scan and X-ray images, The X ray majors have the least value of signal to noise ratio among the category. The MRI images have obtained an snr above 55 dB Whereas the X ray majors have the signal to noise ratio less than 43 dB.

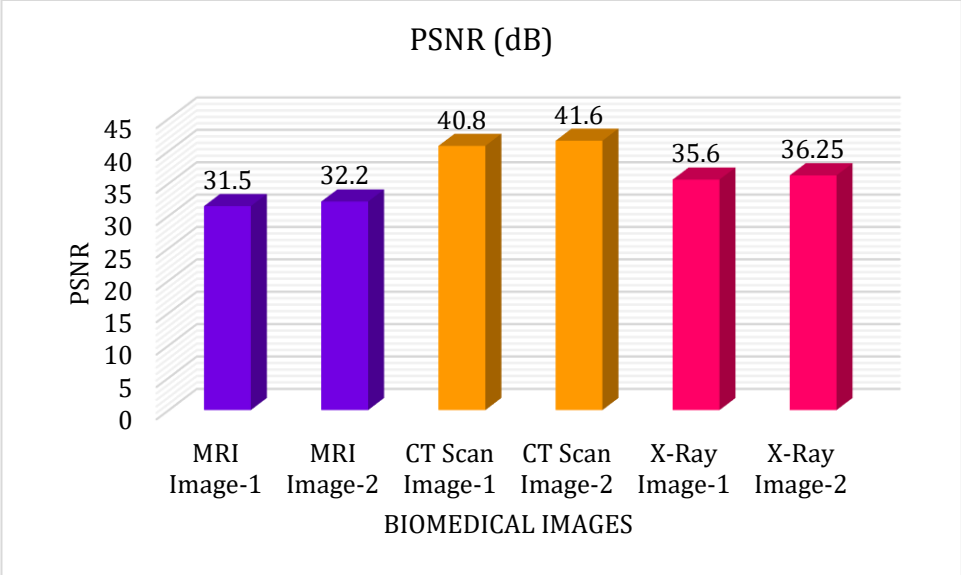

Fig 19: Plot of PSNR for MRI, CT scan and X-ray images.

Figure 19 shows the plot of PSNR for MRI, CT scan and X-ray images. The CT scan images have the highest value of PSNR. The least values are seen in MRI Images. The highest value of PSNR is obtained as 41.6 dB for CT scan image.

With the analysis of the above results it can be concluded that the biomedical image analysis were made with the various parameters so it is observed that MRI image based analysis is the better one for the significant analysis when compared with the other two datasets under consideration. Which helps the medical experts to analyse the patients under consideration.

8. Conclusion.

The comprehensive analysis and evaluation of biomedical imaging samples, specifically focusing on Computed Tomography (CT), X-ray, and Magnetic Resonance Imaging (MRI), utilizing metrics such as True Positive (TP), True Negative (TN), False Positive (FP), False Negative (FN), Sensitivity (Recall rate), Specificity, Precision, and the F1 score, have led to significant insights into the comparative effectiveness of these imaging modalities for disease diagnosis and management. Among these, MRI image samples have demonstrated superior performance in terms of diagnostic accuracy and detail resolution, substantiating their preference for certain clinical applications over CT and X-ray images.

Our findings reveal that MRI samples consistently yield higher TP rates, indicating a superior ability to correctly identify disease presence. This is attributed to MRI's advanced contrast resolution, which allows for the detailed visualization of soft tissues, making it more effective for detecting subtle pathological changes. The TN rates observed with MRI also highlight its effectiveness in accurately confirming the absence of disease, minimizing unnecessary treatments or further diagnostic procedures.

The enhanced Sensitivity (Recall rate) of MRI suggests its superior capability in identifying true positive cases among all actual cases, crucial for early disease detection and intervention. Similarly, the Specificity of MRI indicates its reliability in excluding patients without the disease, reducing the risk of false alarms. Precision and F1 scores further underscore MRI's balanced performance, effectively combining accuracy with consistency in positive predictions and the overall diagnostic process.

Comparatively, while CT and X-ray images are invaluable in various diagnostic scenarios, such as emergency medicine and the evaluation of bone structures, they fall short in areas where soft tissue contrast and detail are paramount. The inherent limitations of CT and X-ray in distinguishing between subtle tissue differences contribute to lower TP rates and potentially higher FP rates, affecting their Sensitivity, Specificity, Precision, and F1 scores relative to MRI.

In conclusion, our study underscores the superior diagnostic capabilities of MRI image samples across a range of performance metrics. MRI's advanced imaging qualities offer unparalleled detail and accuracy, making it the preferred choice for diagnosing and managing conditions requiring high-resolution visualization of soft tissues. While CT and X-ray remain indispensable tools in

the medical imaging arsenal, MRI stands out for its comprehensive and reliable diagnostic performance.

References.

[1] P. Brocken, B. A. Kiers, M. G. Looijen-Salamon et al., "Timeliness of lung cancer diagnosis and treatment in a rapid outpatient diagnostic program with combined 18FDG-PET and contrast enhanced CT scanning," Lung Cancer, vol. 75, no. 3, pp. 336–341, 2012.

[2] P. Vivekanandan, "An efficient SVM based tumor classification with symmetry non-negative matrix factorization using gene expression data," in In 2013 International conference on information communication and embedded systems (Icices), pp. 761–768, IEEE, USA, February 2013.

[3] J. D'Cruz, A. Jadhav, A. Dighe, V. Chavan, and J. Chaudhari, "Detection of lung cancer using backpropagation neural networks and genetic algorithm," Computing Technologies and Applications, vol. 6, pp. 823–827, 2016.

[4] J. Shen, J. Wu, M. Xu, D. Gan, B. An, and F. Liu, "A hybrid method to predict postoperative survival of lung cancer using improved SMOTE and adaptive SVM," Computational and Mathematical Methods in Medicine, vol. 2021, Article ID 2213194, 15 pages, 2021.

[5] S. Mandal and I. Banerjee, "Cancer classification using neural network," International Journal, vol. 172, pp. 18–49, 2015.

[6] D. M. Abdullah, A. M. Abdulazeez, and A. B. Sallow, "Lung cancer prediction and classification based on correlation selection method using machine learning techniques," Qubahan Academic Journal, vol. 1, no. 2, pp. 141–149, 2021.

[7] F. Taher, N. Prakash, A. Shaffie, A. Soliman, and A. El-Baz, "An overview of lung cancer classification algorithms and their performances," IAENG International Journal of Computer Science, vol. 48, no. 4, 2021.

[8] Jaweed and F. Siddiqui, "Implementation of machine learning in lung cancer prediction and prognosis: a review," in Cyber Intelligence and Information Retrieval, pp. 225–231,India, 2022.

[9] V. N. Jenipher and S. Radhika, "SVM kernel methods with data normalization for lung cancer survivability prediction application," in In 2021 Third International Conference on Intelligent Communication Technologies and Virtual Mobile Networks (ICICV), pp. 1294–1299, IEEE, Canada, February 2021.

[10] V. A. Binson, M. Subramoniam, Y. Sunny, and L. Mathew, "Prediction of pulmonary diseases with electronic nose using SVM and XGBoost," IEEE Sensors Journal, vol. 21, no. 18, pp. 20886–20895, 2021.

[11] B. R. Manju, V. Athira, and A. Rajendran, "Efficient multi-level lung cancer prediction model using support vector machine classifier," in In IOP Conference Series: Materials Science and Engineering, vol. 1012, India, 2021no. 1, Article ID 012034IOP Publishing.

[12] P. Nanglia, S. Kumar, A. N. Mahajan, P. Singh, and D. Rathee, "A hybrid algorithm for lung cancer classification using SVM and neural networks," ICT Express, vol. 7, no. 3, pp. 335–341, 2021.

[13] G. Yin, Y. Song, X. Li et al., "Prediction of mediastinal lymph node metastasis based on 18F-FDG PET/CT imaging using support vector machine in non-small cell lung cancer," European Radiology, vol. 31, no. 6, pp. 3983–3992, 2021.

[14] Y. Xie, W.-Y. Meng, R.-Z. Li et al., "Early lung cancer diagnostic biomarker discovery by machine learning methods," Translational Oncology, vol. 14, no. 1, article 100907, 2021.

[15] M. Yakar, D. Etiz, M. Metintas, G. Ak, and O. Celik, "Prediction of radiation pneumonitis with machine learning in stage III lung cancer: a pilot study," Technology in Cancer Research & Treatment, vol. 20, p. 153303382110163, 2021.

[16] N. Maleki, Y. Zeinali, and S. T. A. Niaki, "A k-NN method for lung cancer prognosis with the use of a genetic algorithm for feature selection," Expert Systems with Applications, vol. 164, article 113981, 2021.

[17] S. Vijh, R. Sarma, and S. Kumar, "Lung tumor segmentation using marker-controlled watershed and support vector machine," International Journal of E-Health and Medical Communications (IJEHMC), vol. 12, no. 2, pp. 51–64, 2021.

[18] S. S. Ashwini, M. Z. Kurian, and M. Nagaraja, "Lung cancer detection and prediction using customized selective segmentation technique with SVM classifier," in Emerging Research in Computing, Information, Communication and Applications, pp. 37–44, Springer, Singapore, 2022.

[19] H. A. Miller, X. Yin, S. A. Smith et al., "Evaluation of disease staging and chemotherapeutic response in non-small cell lung cancer from patient tumor-derived metabolomic data," Lung Cancer, vol. 156, pp. 20–30, 2021.

[20] X. Fang, M. Netzer, C. Baumgartner, C. Bai, and X. Wang, "Genetic network and gene set enrichment analysis to identify biomarkers related to cigarette

smoking and lung cancer," Cancer Treatment Reviews, vol. 39, no. 1, pp. 77–88, 2013.

[21] N. L. Guo and Y. W. Wan, "Pathway-based identification of a smoking associated 6-gene signature predictive of lung cancer risk and survival," Artificial Intelligence in Medicine, vol. 55, no. 2, pp. 97–105, 2012.

[22] V. Krishnaiah, G. Narsimha, and N. S. Chandra, "Diagnosis of lung cancer prediction system using data mining classification techniques," International Journal of Computer Science and Information Technologies, vol. 4, no. 1, pp. 39–45, 2013.

[23] C. Anil Kumar et al, "Lung Cancer Prediction from Text Datasets Using Machine Learning " , Hindawi BioMed Research International Volume 2022, Article ID 6254177, 10 pages https://doi.org/10.1155/2022/6254177

[24] K. Polat and S. Güneş, "Principles component analysis, fuzzy weighting pre-processing and artificial immune recognition system based diagnostic system for diagnosis of lung cancer," Expert Systems with Applications, vol. 34, no. 1, pp. 214–221, 2008.

[25] Y. Qian, Y. Zhang, X. Ma, H. Yu, and L. Peng, "EARS: emotion-aware recommender system based on hybrid information fusion," Information Fusion, vol. 46, pp. 141–146, 2019.

[26] Y. Shin and J. Ghosh, "Ridge polynomial networks," IEEE Transactions on Neural Networks, vol. 6, no. 3, pp. 610–622, 1995.

[27] F. Taher and R. Sammouda, "Lung cancer detection by using artificial neural network and fuzzy clustering methods," in In 2011 IEEE GCC conference and exhibition (GCC), pp. 295–298, IEEE, United Arab Emirates, February 2011.

[28] Q. N. Tran, "A novel method for finding non-small cell lung cancer diagnosis biomarkers," BMC Medical Genomics, vol. 6, Supplement 1, p. S11, 2013.

[29] T. Kaur and N. Gupta, "Classification of lung diseases using particle swarm optimization," International Journal of Advanced Research in Electronics and Communication Engineering, vol. 4, no. 9, pp. 2440–2446, 2015.

[30] S. Xiao, H. Yu, Y. Wu, Z. Peng, and Y. Zhang, "Self-evolving trading strategy integrating internet of things and big data," IEEE Internet of Things Journal, vol. 5, no. 4, pp. 2518–2525, 2018.

[31] Y. Zhang, R. Gravina, H. Lu, M. Villari, and G. Fortino, "PEA: parallel electrocardiogram-based authentication for smart healthcare systems," Journal of Network and Computer Applications,vol. 117, pp. 10–16, 2018.

[32] Y. Zhang, Z. Tu, and Q. Wang, "TempoRec: temporal-topic based recommender for social network services," Mobile Networks and Applications, vol. 22, no. 6, pp. 1182–1191, 2017.